

# Conformational Transitions of Amyloid- $\beta$ : A Langevin and Generalized Langevin Dynamics Simulation Study

Vishal Singh and Parbati Biswas\*

Cite This: *ACS Omega* 2021, 6, 13611–13619

Read Online

ACCESS |



Metrics &amp; More

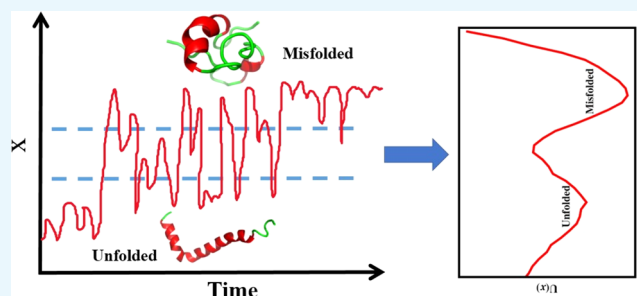


Article Recommendations



Supporting Information

**ABSTRACT:** The dynamics of conformational transitions of the disordered protein, amyloid- $\beta$ , is studied via Langevin and generalized Langevin dynamics simulations. The transmission coefficient for the unfold–misfold transition of amyloid- $\beta$  is calculated from multiple independent trajectories that originate at the transition state with different initial velocities and are directly correlated to Kramers and Grote–Hynes theories. For lower values of the frictional coefficient, a well-defined rate constant is obtained, whereas, for higher values, the transmission coefficient decays with time, indicating a breakdown of the Kramers and Grote–Hynes theories and the emergence of a dynamic disorder, which demonstrates the presence of multiple local minima in the misfolding potential energy surface. The calculated free energy profile describes a two-state transition of amyloid- $\beta$  in the energy landscape. The transition path time distribution computed from these simulations is compared with the related experimental and theoretical results for the unfold–misfold transition of amyloid- $\beta$ . The high free energy barrier for this transition confirms the misfolding of amyloid- $\beta$ . These findings offer an insight into the dynamics of the unfold–misfold transition of this protein.



## 1. INTRODUCTION

The functional specificity of proteins is intricately linked to various cooperative conformational transitions that govern both beneficial cellular processes like folding, signaling, transport, and allostery catalysis and the detrimental ones such as misfolding and aggregation. Such conformational transitions span a wide range of time scales typically from microseconds to seconds and even longer.<sup>1–3</sup> A description of the folding energy landscape of a protein requires the complete specification of the conformational and dynamic properties of each state. For most proteins, the native conformation is well defined, while much less is known about the sparsely populated non-native ensemble, which includes the misfolded states.<sup>4,5</sup> Different experimental and computational techniques that complement each other to characterize the structure and conformational dynamics at different resolutions and across different time scales include neutron scattering, NMR, Mossbauer spectroscopy, dielectric spectroscopy, differential scanning calorimetry, X-ray crystallography, and molecular dynamics simulations.<sup>6–11</sup> However, the experimental/simulation data typically measure the ensemble-averaged conformational and dynamic properties of these structural transitions. Computer simulations provide a molecular insight into protein dynamics over a wide range of spatial and temporal resolutions. Such studies are especially useful as they differentiate between the functional native structure from the dysfunctional misfolded ones.

Misfolded proteins are aggregate-prone and self-assemble to form different types of aggregates ranging from oligomers to  $\beta$ -rich insoluble amyloid fibrils/plaques. Numerous debilitating neurodegenerative disorders such as Alzheimer's disease, Parkinson's disease, Huntington's disease, and amyotrophic lateral sclerosis (ALS) are caused by the formation of these aggregates/fibrils. The amyloid- $\beta$  peptide, which is an intrinsically disordered protein, is the principal component of the amyloid deposits in Alzheimer's disease. The energy landscape of disordered proteins has several local minima separated by small energy barriers. The transition between these states generates an ensemble of multiple structurally dissimilar states, which have approximately equal energy.<sup>12</sup> Such states constitute the misfolded conformational ensemble, and the conformational transition of amyloid- $\beta$  may be considered as two-state transition from the natively unfolded to the misfolded state in the free energy landscape.<sup>13,14</sup> Many experimental and simulation studies have investigated the conformational transitions of the full-length amyloid- $\beta$  to characterize the misfolding of this protein in water<sup>13–15</sup> using

Received: January 28, 2021

Accepted: May 10, 2021

Published: May 19, 2021



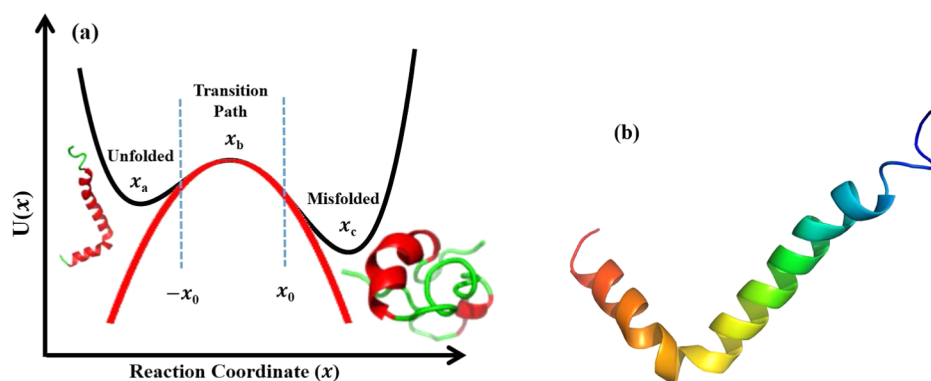


**Figure 1.** (a) Schematic of the transition path that corresponds to the unfold–misfold transition of protein within the confined domain  $-x_0 < x_b < x_0$  without crossing the boundaries. (b) NMR structure of amyloid- $\beta$  42 monomer (PDB ID: 1IYT).

both implicit and explicit solvent models. The conversion of amyloid- $\beta$  from an  $\alpha$  helix or random coil structure to a  $\beta$  sheet is typically associated with the onset of disease. However, an understanding of the dynamics of the complex conformational transitions that span over different time scales requires an examination of each individual transition rather than an averaged one obtained from the entire ensemble of conformations. Stochastic dynamics simulations are a powerful tool to characterize the conformational dynamics of proteins by analyzing their transition paths.<sup>16</sup> A transition path corresponds to an infinitesimal part of the molecular trajectory where the molecule crosses the transition state within a confined domain across a potential barrier separating the conformations<sup>17,18</sup> (see Figure 1a). Such a path contains key microscopic information about the structural transitions that may be probed by high-resolution single-molecule experiments and all-atom simulations.

This study probes the dynamics of conformational transitions of amyloid- $\beta$  in implicit water through all-atom Langevin dynamics (LD) and generalized Langevin dynamics (GLD) simulations. The helical structure of the full-length amyloid- $\beta$  as determined by NMR in a mixture of water and organic solvent was selected as an initial template for this natively unfolded protein<sup>13–15</sup> (see Figure 1b). The rate of conformational transitions is proportional to the transmission coefficient. The time-dependent transmission coefficient is evaluated from multiple independent simulation trajectories of amyloid- $\beta$ . Results of the transmission coefficients with varying strengths of friction are directly correlated with Kramers and Grote–Hynes rate theories.<sup>19–22</sup> In the high friction limit, the conformational transition from the natively unfolded to a misfolded state violates both Kramers and Grote–Hynes rate theories with the emergence of a dynamic disorder in the system, which indicates the presence of multiple local minima in the misfolding potential energy surface. The dynamics of this unfold–misfold transition of amyloid- $\beta$  is studied by analyzing the one-dimensional free energy profile (FEP) and the transition path. The time required to traverse the transition path known as transition path time (TPT) or mean transition path time (MTPT) is estimated from both LD and GLD simulations. The distribution of the transition path times is also calculated by varying the width of the transition region and is compared to the theoretically obtained results, which provide the height and frequency of the potential barrier for such a transition of amyloid- $\beta$ . The high free energy barrier for this transition confirms the misfolding of amyloid- $\beta$ . These

findings offer an insight into the dynamics of the unfold–misfold transition of amyloid- $\beta$ .

## 2. METHODS

**2.1. Computational Details.** The dynamics of the conformational transition of full-length amyloid- $\beta$  ( $A\beta$ 42, PDB code: 1IYT) is investigated via all-atom Langevin and generalized Langevin dynamics (LD and GLD) simulations in implicit water. The LD and GLD simulations are performed using AMBER 18 suite of programs<sup>23</sup> with ff99SBildn<sup>24,25</sup> force field at a temperature of 300 K. The temperature was kept constant throughout the simulations using a Langevin thermostat.<sup>26</sup> Initially, the energy of the system was minimized in two steps using the steepest descent and conjugate gradient methods to remove the unfavorable interactions. For the implicit solvent simulations, the OBC variant (*igb5*) of the generalized Born (GB) method is used with the effective Born radii, *rgbmax* = 15.0 Å. We used counterions of 0.1 M salt in the simulation for GB implicit solvent. The solvation free energy includes the respective contributions of the electrostatic and nonpolar interactions that are estimated from the generalized Born model<sup>27,28</sup> and the solvent-accessible surface area.<sup>29</sup> The energy-minimized  $A\beta$  protein was equilibrated for 100 ps, while the temperature is increased from 0 to 300 K. This step is followed by the equilibration of the system for 5 ns without any periodic boundary conditions, in which the constraint on  $A\beta$  is relaxed gradually. SHAKE algorithm<sup>30</sup> is used for constraining the motion of the hydrogen atoms at their respective equilibrium bond lengths. The equilibrated protein is subjected to the final production run, where all restraints are removed. The coordinates of all atoms were recorded at every 2 ps. A total of 100 independent LD simulations (each of 5 ns) and 500 independent GLD simulations (each of 2.5 ns) of  $A\beta$  with different initial random velocities were performed to improve the resolution of the time autocorrelation functions and the transmission coefficients for the conformational transitions of  $A\beta$ . The free energy profile (FEP), transition path time distribution (TPTD), and the mean transition path times (MTPT) are calculated from single trajectories of 360 ns for each of LD and GLD simulations. The root-mean-square deviation (RMSD) and radius of gyration ( $R_g$ ) of amyloid- $\beta$  from the LD and GLD simulations at different values of frictional coefficient,  $\gamma$ , are given in the Supporting Information (see Figures S1 and S2).

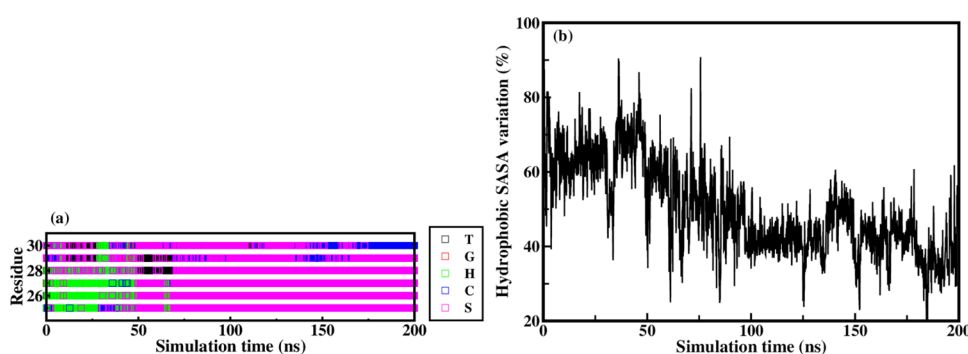


**Figure 2.** Time evolution of the (a) formation of a hydrophilic loop between the residues 25 and 29 and (b) change in SASA of the hydrophobic regions of  $A\beta$  protein from its initial structure. Here, H, G, S, T, and C denote  $\alpha$ -helix,  $3_{10}$ -helix, bend, hydrogen-bonded turn, and random coil, respectively.

The LD simulation is based on the classical Langevin equation,<sup>31</sup> which is given by

$$m\ddot{x}(t) = -U'(x) - m\gamma\dot{x}(t) + \xi(t) \quad (1)$$

where  $m$  and  $x(t)$  are the mass and position of the protein, respectively;  $U(x)$  is the potential; and  $\gamma$  is the frictional coefficient that measures the strength of friction/interaction between the amyloid- $\beta$  and water molecules. The random force is modeled by the Gaussian white noise,  $\xi(t)$ , with a zero mean  $\langle \xi(t) \rangle = 0$  and delta correlation according to the fluctuation–dissipation theorem<sup>31</sup> (FDT) as  $\langle \xi(t)\xi(t') \rangle = 2mk_{\text{B}}T\delta(t - t')$ , where  $k_{\text{B}}$  is the Boltzmann constant and  $T$  is the absolute temperature.

The GLD simulation is based on the generalized Langevin equation<sup>31,32</sup> (GLE), which is given as

$$m\ddot{x}(t) = -U'(x) - m \int_0^t \gamma(t - t')\dot{x}(t')dt' + \xi(t) \quad (2)$$

where  $\gamma(t - t')$  is the time-dependent frictional memory kernel, which is related to  $\xi(t)$  through the FDT<sup>31,33</sup> as:  $\langle \xi(t)\xi(t') \rangle = mk_{\text{B}}T\gamma(t - t')$ . The time-dependent frictional memory kernel in AMBER 18 is given by  $2\delta(t) - \frac{\lambda}{t_{\text{L}}}e^{-t/t_{\text{L}}}$ , where  $\lambda$  is the strength of the frictional force and  $t_{\text{L}}$  is the memory time for the non-Markovian dynamics.

All-atom molecular dynamics (MD) simulation with explicit solvent is also performed using AMBER 18 suite of programs<sup>23</sup> with ff99SBildn<sup>24</sup> force field at a constant temperature of 300 K. The temperature is kept constant throughout the simulation using a Berendsen thermostat<sup>34</sup> with a coupling constant of 1.0 ps. The initial helical structure of  $A\beta$  is solvated in TIP3P water in a rectangular box of  $56.0 \times 46.5 \times 73.6 \text{ \AA}^3$ , where the distance between the edge of the box and  $A\beta$  is kept sufficiently large, i.e., 10.0  $\text{\AA}$ , and the periodic boundary condition is applied. Counterions  $\text{Na}^+$  are added to neutralize the overall charge of  $A\beta$ . The energy of the system is minimized, followed by the equilibration steps where the temperature is increased from 0 to 300 K. The long-range electrostatic interactions are treated using the particle mesh Ewald (PME) algorithm<sup>35</sup> with a cutoff of 8.0  $\text{\AA}$ . After the equilibration run, the final MD simulation is performed for 310 ns in an NPT ensemble, where the coordinates of all atoms are recorded at every 2 ps. The FEP, TPTD, and MTPT are calculated for the conformational transition of  $A\beta$  from the MD simulation trajectory.

**2.2. Misfolding in Amyloid- $\beta$ .** The wild-type full-length  $A\beta$  42 (PDB code: 1IYT) is chosen as an initial structure for

the LD and GLD simulations (see Figure 1b). This structure is commonly used in molecular dynamics (MD) simulations to characterize the conformational transitions of  $A\beta$ .<sup>13–15</sup> We explore the conformational transitions and identify the misfolding of this protein with LD and GLD simulations in implicit water. The study of the conformational transition of  $A\beta$  from the unfolded state (U) to the misfolded state (M) is reported in the literature,<sup>13,14</sup> where the misfolding is characterized by (i) the formation of a hydrophilic loop between the residues 25 and 29, and (ii) the proximity of the central hydrophobic core region (residues 17–21) and the C-terminus. Figure 2a displays the time evolution of formation of a hydrophilic loop between the residues 25 and 29 of  $A\beta$ . The native helical structure between residues 25 and 29 (see Figure 1b) in  $A\beta$  is disrupted and converted to a loop (shown in magenta boxes) with time. Thus,  $R_{\text{g}}$  of  $A\beta$  decreases gradually and the protein becomes more compact. Figure 2b shows the time evolution of the hydrophobic solvent-accessible surface area (SASA) for the hydrophobic regions (17–21) of  $A\beta$ . The variation of SASA of the hydrophobic regions is reflected in the fluctuation of the C-terminal residues of  $A\beta$ . An increase in SASA is observed when the hydrophobic regions are away from the C-terminal regions. However, a decrease in SASA represents that the hydrophobic residues 17–21 are closer to the C-terminal regions.<sup>14</sup> These two regions, i.e., hydrophobic and C-terminal regions, come closer due to the formation of the hydrophilic loop between the residues 25 and 29. It is also noticed that there is no salt bridge between residues 23 and 28, which is in agreement with earlier studies.<sup>14,36</sup> These observations characterize the misfolding events of  $A\beta$ .<sup>13,14</sup> The dynamics of the conformational transitions of  $A\beta$  is studied by calculating the transmission coefficient, distribution of the transition path times, free energy profile, and the mean transition path times.

### 3. RESULTS AND DISCUSSION

**3.1. Transmission Coefficients.** The rate constant,  $k_{\text{TST}}$ , in the transition state theory (TST) is calculated on the assumption that there is no recrossing of the trajectory once it crosses the transition state.<sup>37,38</sup> But according to Eyring,<sup>39</sup> recrossing may occur and the protein may revert back to its original unfolded state. A time-dependent transmission coefficient,  $\kappa(t)$ , is introduced to compensate for these recrossings as

$$k(t) = \kappa(t)k_{\text{TST}} \quad (3)$$

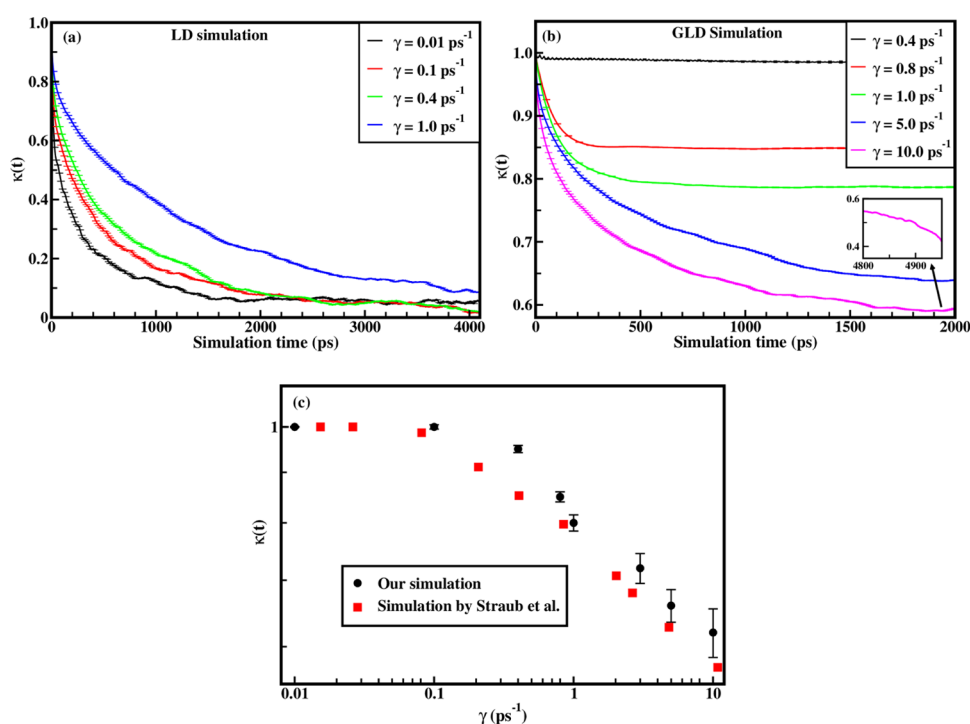


**Figure 3.** Time-dependent transmission coefficient,  $\kappa(t)$ , versus simulation time with varying values of  $\gamma$  for (a) LD and (b) GLD simulations. The transmission coefficients calculated from the LD and GLD simulations are averaged over 100 and 500 independent trajectories, respectively. The plateau value of  $\kappa(t)$  indicates a well-defined rate constant for the unfold–misfold transition of  $A\beta$ , whereas the absence of plateau shows the emergence of a dynamic disorder. (c) Comparison of  $\kappa(t)$  with the simulation data obtained by Straub et al.<sup>46</sup> The error bars show the standard errors obtained by averaging over multiple independent trajectories.

where  $k(t)$  is the rate of the unfold–misfold transition of  $A\beta$  and  $\kappa(t)$  is calculated from the LD and GLD simulations averaged over multiple independent trajectories of  $A\beta$  with different initial velocities, assuming that the initial position of  $A\beta$  is at the transition state. The transition state is close to the plane that corresponds to the maximum of the FEP along the reaction coordinate,  $x(t)$  (i.e., RMSD of the protein). Therefore, the conformation of the protein that corresponds to the saddle point of the FEP is chosen as a transition state because it has equal probability to cross the barrier toward either side of the potential well, i.e., unfolded or misfolded state.<sup>40,41</sup> The calculation of the time-dependent transmission coefficient is based on each trajectory and the time autocorrelation function. The time autocorrelation function,  $C(t)$ , for the conformational fluctuations of  $A\beta$  may be defined as<sup>42</sup>

$$C(t) = \frac{\langle \delta N_U(0) \delta N_U(t) \rangle}{\langle \delta N_U(0) \delta N_U(0) \rangle} \quad (4)$$

where  $\delta N_U(t) = N_U(t) - \langle N_U \rangle$  and  $N_U$  is the number of trajectories in the unfolded region (i.e., left of the transition state) of  $A\beta$  at time  $t$ , which is given by

$$N_U(t) = \sum_i \theta(x_i^\ddagger - x_i(t)) \quad (5)$$

where  $x_i^\ddagger$  is the position of the transition state, which represents a saddle point at the top of the barrier that divides the potential surface between the unfolded and misfolded basins, and  $x_i(t)$  denotes the position of the protein along the reaction coordinate at time  $t$ . The reaction coordinate,  $x(t)$ , corresponds to the root-mean-square deviation (RMSD) of the

protein with respect to its initial structure.<sup>25</sup>  $\theta(x(t))$  denotes an unit step function

$$\theta(x_i^\ddagger - x_i(t)) = \begin{cases} 1; & x_i^\ddagger \geq x_i(t) \\ 0; & x_i^\ddagger < x_i(t) \end{cases}$$

The brackets  $\langle \bullet \rangle$  denote the statistical averaging over all of the trajectories. The plot of the normalized time autocorrelation function,  $C(t)$ , versus time,  $t$ , for the LD and GLD simulations are shown in Figure S3a,b in the Supporting Information, respectively. At initial times, a maximum value of normalized  $C(t)$  indicates the initial position of  $A\beta$  at the saddle point. As expected from eq 4,  $C(t)$  decreases exponentially with time, which denotes the positional fluctuations of  $A\beta$  from its initial state, i.e., unfolded state. The decay of  $C(t)$  as a function of  $t$  indicates two different types of motion of  $A\beta$ . Initially,  $C(t)$  decays rapidly (around 1500 ps for LD and 500 ps for GLD simulation) as  $A\beta$  misfolds. Consequently,  $C(t)$  becomes constant. The time autocorrelation function may be fitted to a stretched exponential function  $C(t) = \sum_{i=1}^2 C_i \exp\left[-\left(\frac{t}{\tau_i}\right)^{\alpha_i}\right]$ . Here,  $\tau$  is the relaxation time and  $\alpha$  is the stretched exponent for the fit of  $C(t)$ . The time-dependent transmission coefficient,  $\kappa(t)$ , for the unfold–misfold transition of  $A\beta$  is calculated from the reactive flux formalism as postulated by Chandler.<sup>42–45</sup>  $\kappa(t)$  is given as

$$\kappa(t) = \frac{\langle \delta(x(0) - x^\ddagger) \dot{x}(0) \theta(x(t) - x^\ddagger) \rangle}{\langle \delta(x(0) - x^\ddagger) \dot{x}(0) \theta(x(0) - x^\ddagger) \rangle} \quad (6)$$

where  $\dot{x}(0)$  is the initial velocity of the trajectory, which is calculated from the simulation data. The transmission

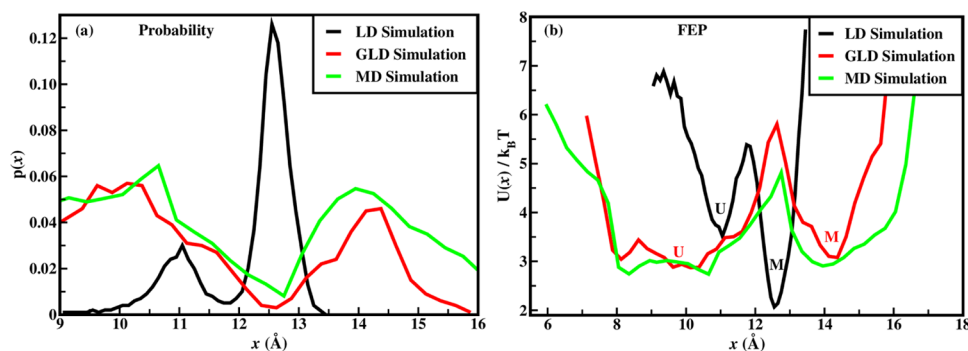


**Figure 4.** (a) Probability distribution of the conformations and (b) one-dimensional FEP ( $-\ln(p(x))$ ) for the unfold–misfold transition of  $A\beta$  from LD, GLD, and MD simulations. The FEP is described as a two-state transition (unfold–misfold) of  $A\beta$  in a free energy landscape. Here, U and M denote the unfolded and misfolded states of  $A\beta$  respectively.  $x$  corresponds to RMSD of the protein.

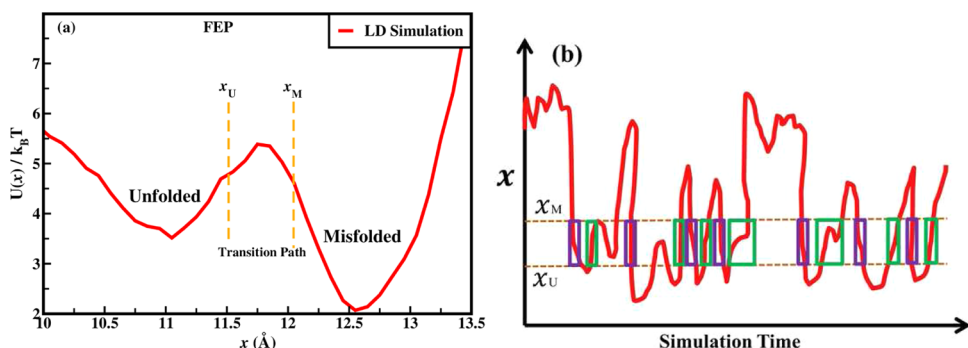


**Figure 5.** (a) Transition path and (b) schematic diagram of the trajectory in small simulation time for the conformational transitions of  $A\beta$ .  $x_U$  and  $x_M$  are the boundaries for the unfolded and misfolded states, respectively. The region between orange lines shows the transition path, where purple boxes depict misfold–unfold transitions, and green boxes show unfold–misfold transitions of  $A\beta$ .

coefficients calculated from the LD and GLD simulations are averaged over 100 and 500 independent trajectories, respectively, for different values of the frictional coefficient,  $\gamma$ . Figure 3a,b portrays the time-dependent  $\kappa(t)$  for the unfold–misfold transition of  $A\beta$  calculated from eq 6 using LD and GLD simulations, respectively, with varying values of  $\gamma$ . The transmission coefficients,  $\kappa(t)$ , usually vary between 0 and 1. At time  $t = 0$ ,  $\kappa(t) \sim 1$ , which indicates that initially there is no unfold–misfold transition and this corresponds to the ideal case of TST. Figure 3a shows that  $\kappa(t)$  decreases monotonically with time and ultimately vanishes with increasing  $\gamma$ .  $\kappa(t)$  calculated from the LD simulations follows the Kramers theory.<sup>19,20,22</sup> The Kramers theory based on the Langevin equation is Markovian, i.e., it does not account for the memory effects as the random forces are uncorrelated in time and do not accurately account for the solvent forces at small times due to the complex protein–solvent interactions.<sup>22,47</sup> However, the motion of the protein induces memory effects in the system, which affects its dynamics in solutions. Thus,  $\kappa(t)$  for the unfold–misfold transition of  $A\beta$  is not well defined in LD simulations. In Figure 3b,  $\kappa(t)$  decays rapidly at small times as  $A\beta$  misfolds, but after a certain time,  $\kappa(t)$  plateaus off, which represents the existence of a well-defined rate constant for the conformational transitions of  $A\beta$ . However,  $\kappa(t)$  obtained from the GLD simulations follows the Grote–Hynes rate theory,<sup>21,22</sup> which is based on the GLE (non-Markovian) that accounts for the memory effects in the system, where the random forces are correlated in time. This non-Markovian nature of the system is expected to play a significant role in the conformational transition of the protein, and hence the GLD

simulation provides a better description of the dynamics of the unfold–misfold transition of  $A\beta$ . The GLD simulation accurately describes the transmission coefficients for different values of the frictional coefficient. At very low values of the frictional coefficients (i.e.,  $\gamma = 0.1$  and  $0.4 \text{ ps}^{-1}$ ), the unfold–misfold transition does not occur, and therefore the maximum value of  $\kappa(t)$  is unity, whereas, for high values of  $\gamma$  (i.e.,  $\gamma = 5$  and  $10 \text{ ps}^{-1}$ ),  $A\beta$  shows conformational fluctuations in the misfolded state that gives rise to multiple local minima in the misfolding potential energy surface. The transitions of the misfolded  $A\beta$  protein from one local minima to another may affect the rate of the unfold–misfold transition. Thus,  $\kappa(t)$  decreases and does not reach a plateau with time, which indicates an absence of a well-defined rate constant. The absence of the plateau confirms the breakdown of the Kramers and Grote–Hynes rate theories and indicates the presence of dynamic disorder in the conformational transitions of  $A\beta$ , which is similar to the earlier experimental and simulation studies on the conformational fluctuations of single protein molecules.<sup>48–50</sup> These studies also suggest that dynamic disorder arising due to the conformational transitions spans a wide range of time scales rather than mere fluctuations in the barrier height. Figure 3c displays a log–log plot of  $\kappa(t)$  versus  $\gamma$ , which shows a good agreement of our results with the simulation data of Straub et al.<sup>46</sup>

**3.2. Free Energy Profile (FEP).** The FEP and the transition path for the unfold–misfold transition may be calculated from the LD and GLD simulations. The FEP is described as<sup>16</sup>

$$U(x) = -k_B T \ln(p(x)) \quad (7)$$

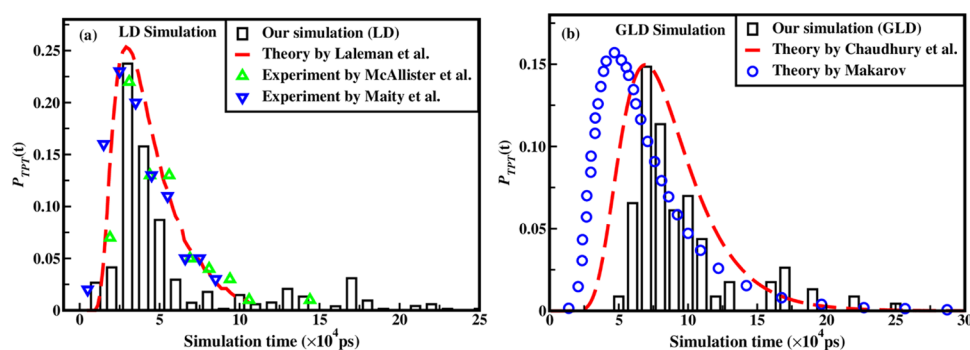


**Figure 6.** TPTD,  $P_{\text{TPT}}(t)$ , versus simulation time for (a) LD and (b) GLD simulations. Comparison of  $P_{\text{TPT}}(t)$  obtained from (a) our LD simulation with the experimental results of TPTD for  $A\beta$ <sup>52,53</sup> and with an earlier theory<sup>54</sup> and (b) our GLD simulation with the theoretical results.<sup>16,55</sup>

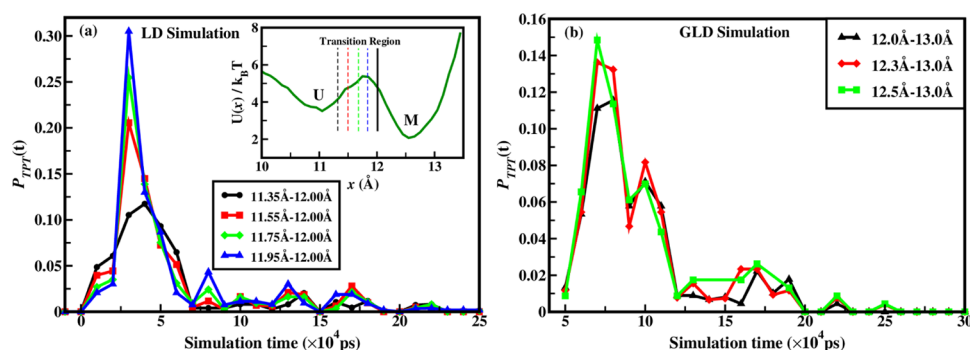


**Figure 7.** TPTD,  $P_{\text{TPT}}(t)$ , versus simulation time with varying width of the transition region for (a) LD and (b) GLD simulations.

where  $p(x)$  denotes the probability distribution along the reaction coordinate,  $x(t)$ , for the unfold–misfold transition of  $A\beta$ , where the reaction coordinate corresponds to the root-mean-square deviation (RMSD) of the protein with respect to its initial structure.<sup>25</sup> Figure 4a,b presents the probability distribution of the conformations,  $p(x)$  and  $-\ln(p(x))$  (FEP), respectively, for the unfold–misfold transition of  $A\beta$  from LD, GLD, and MD simulations. The potential obtained from these simulation data may be viewed as a two-state transition (unfold–misfold) of  $A\beta$  in a free energy landscape. The misfolded state of  $A\beta$  occurs as a narrow well located on the right-hand side of the free energy landscape. While the unfolded state is relatively broad and appears on the left-hand side of this free energy landscape. Thus, Figure 4b exhibits a broad unfolded basin and a narrow misfolded basin. The energy landscape of such transitions is typically rugged, which indicates several closely spaced conformations that belong to the unfolded and misfolded states. Therefore, the unfold–misfold transition may occur in a heterogeneous manner.<sup>51</sup> The dynamics of this conformational transition may be investigated by analyzing the transition path between the unfolded and misfolded states. Two boundaries  $x_U$  and  $x_M$  may be arbitrarily defined between these states, where the position  $x < x_U$  corresponds to the unfolded state and the position  $x > x_M$  represents the misfolded state of  $A\beta$ . The region defined between  $x_U \leq x \leq x_M$  represents the conformation of  $A\beta$  in the transition state as it enters from one side of this interval and exits from the other.  $A\beta$  continuously dwells inside this region as depicted in Figure 5a,b when the choice of this transition region is arbitrary. We explore the temporal duration of this transition path known as transition path time (TPT) or the transit time by analyzing this transition region between

unfolded and misfolded states of  $A\beta$ . Figure S6a,b in the Supporting Information depicts the free energy profile (FEP) with varying values of the frictional coefficients,  $\gamma$ , for both LD and GLD simulations.

**3.3. Transition Path Time Distribution (TPTD).** The calculated TPTD,  $P_{\text{TPT}}(t)$ , for the conformational transition of  $A\beta$  obtained from LD and GLD simulations is depicted in Figure 6a,b, respectively.  $P_{\text{TPT}}(t)$  is computed directly from the simulation trajectories by calculating the number of these transition events between the unfolded and misfolded states. Initially, higher values of  $P_{\text{TPT}}(t)$  are obtained as unfold–misfold transition is more frequent, but with increasing times,  $P_{\text{TPT}}(t)$  decreases as the protein misfolds. In the long time limit,  $P_{\text{TPT}}(t)$  becomes zero, indicating that the protein is completely misfolded.  $P_{\text{TPT}}(t)$  calculated from the LD simulation trajectory is compared with the experimental results of TPTD for the  $A\beta$ <sup>52,53</sup> and with an earlier theory.<sup>54</sup> Figure 6a depicts a plot of  $P_{\text{TPT}}(t)$  versus  $t$ , obtained from our LD simulation with the theoretical result of Laleman et al.<sup>54</sup> The theoretical expression of the TPTD based on classical Langevin equation with Gaussian white noise is given as<sup>54</sup>

$$P_{\text{TPT}}(t) = -\frac{2}{\sqrt{\pi}} \frac{G'(t)e^{-G^2(t)}}{1 - \text{Erf}(\sqrt{\beta\Delta E})} \quad (8)$$

where  $G' = dG/dt$  is the time derivative of  $G(t) = \frac{x_0 - X_0(t)}{\sqrt{2\sigma^2(t)}}$  and  $\Delta E$  is the height of the potential barrier.  $X_0(t)$  denotes the deterministic motion of the protein molecule from its initial position  $x(0) = x_0$ . In this context, our simulation results are compared with the data extracted from the atomic force microscopy experiments.<sup>52,53</sup> Results of our simulation qualitatively agree with the experimental and theoretical

results. Figure 6b shows a comparison of  $P_{\text{TPT}}(t)$  versus  $t$ , obtained from our GLD simulation data with the results obtained from theory.<sup>16,55,56</sup> The equation of the TPTD for the transit across harmonic potential barrier obtained by Chaudhury and Makarov<sup>55</sup> is given by

$$P_{\text{TPT}}(t) = \frac{\omega\sqrt{\beta\Delta E}}{1 - \text{Erf}\sqrt{\beta\Delta E}} \frac{\exp[-\beta\Delta E \coth(\omega t/2)]}{\sinh(\omega t/2)\sqrt{2\pi} \sinh(\omega t)} \quad (9)$$

This equation is used for fitting the histograms of the TPTD obtained from our GLD simulations. The values of the height,  $\Delta E = 6.5k_{\text{B}}T$ , and frequency,  $\omega = 0.38 \text{ s}^{-1}$ , of the potential barrier for the unfold–misfold transition of  $A\beta$  are obtained from such a fit.<sup>55</sup> The estimated free energy barrier for unfold–misfold transition of  $A\beta$  is found to be high, i.e.,  $\beta\Delta E \gg 1$ , while the barrier frequency is considerably small.<sup>51,57</sup> The deviation of the TPTD from the theoretical result obtained by Makarov et al.<sup>16</sup> is due to the inclusion of the inertial term in the GLD simulations. While our simulations are based on the inertial GLE, the results of Makarov et al. are derived from the overdamped GLE. Figure S7a in the Supporting Information shows the plot of the TPTD,  $P_{\text{TPT}}(t)$ , versus simulation time in the MD simulation of  $A\beta$ .

Figure 7a,b displays  $P_{\text{TPT}}(t)$  calculated by varying the width of the transition region between the unfolded and misfolded states for both LD and GLD simulations, respectively. Longer transition paths require a longer rearrangement of the protein chain that increases the effective friction between the protein and the solvent along the reaction coordinate, and retarding the motion of the protein.<sup>16</sup> Thus, as the width of the transition region increases, the frequency of crossing the barrier top decreases and hence a lower TPTD is obtained. The plots of the TPTD with varying widths of the transition region show a similar trend to that of an earlier simulation study of binding of intrinsically disordered proteins.<sup>16</sup>

Figure 8 shows the plot of  $P_{\text{TPT}}(t)$  for LD simulation of  $A\beta$  with varying values of the frictional coefficient. For lower

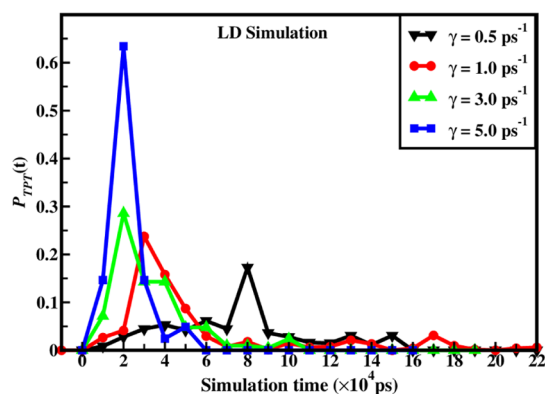


**Figure 8.** TPTD,  $P_{\text{TPT}}(t)$ , obtained from the LD simulation with varying values of frictional coefficient,  $\gamma$ .

frictional strengths, the interactions between  $A\beta$  and the water molecules are less; therefore, there are less transitions between the unfolded and misfolded states, which is reflected in a lower distribution of the transition path times. However, for higher frictional strengths, there are strong interactions between  $A\beta$  and the water molecules. Thus, the conformation of  $A\beta$  is strongly influenced by the thermal noise, which leads to

multiple crossings of the transition-region boundaries, and hence a higher distribution of TPT is obtained.

**3.4. Mean Transition Path Times (MTPT).** Figure 9a,b depicts the MTPT,  $\langle t_{\text{TP}} \rangle$ , as a function of the width of the transition region for LD and GLD simulations, respectively. MTPT measures the average time spent by amyloid- $\beta$  in the transition region ( $x_{\text{U}} \leq x \leq x_{\text{M}}$ ) during the transition from the unfolded state (i.e.,  $x_{\text{U}}$ ) to the misfolded state (i.e.,  $x_{\text{M}}$ ) (see Figure 5b).<sup>16</sup> The transition-region boundaries are self-determined by physical considerations, where the difference of these boundaries may be defined as  $\Delta x = x_{\text{M}} - x_{\text{U}}$ . The MTPT of the unfold–misfold transition of  $A\beta$  decreases as the width of the transition region,  $\Delta x$ , decreases, which implies that the protein spends less time between the transition boundaries. Figure S7b in the Supporting Information shows the plot of MTPT,  $\langle t_{\text{TP}} \rangle$ , versus the width of the transition region in the MD simulation of  $A\beta$ .

## 4. CONCLUSIONS

In this study, we aim to investigate the dynamics of conformational transitions of amyloid- $\beta$  via Langevin and generalized Langevin dynamics (LD and GLD) simulations. LD is based on the classical Langevin equation, while GLD follows the GLE with a non-Markovian frictional memory kernel. The dynamics of the unfold–misfold transition of amyloid- $\beta$  are studied by analyzing the position of  $A\beta$  with time and varying friction strengths of the solvent. The transmission coefficient is calculated via sampling multiple independent trajectories of  $A\beta$  that begin from the transition state with different initial velocities. The calculated transmission coefficients from the LD and GLD simulation data for different frictional coefficients exactly follow the Kramers and Grote–Hynes rate theories, respectively. The transmission coefficient decreases monotonically with time and eventually goes to zero for all values of the frictional coefficient in LD simulations. The non-Markovian nature of the system plays a significant role in the conformational transition of proteins as the motion of protein induces memory effects, which affects its dynamics in the solution. Therefore, the GLD simulation provides a better description of the dynamics of the unfold–misfold transition of  $A\beta$  and accurately describes the transmission coefficients for different values of the frictional coefficient. For lower values of the frictional coefficient, a well-defined rate constant is obtained from the GLD simulations, whereas for higher values of the frictional coefficient, the transmission coefficient decays with time, which indicates the failure/breakdown of the Kramers and Grote–Hynes theories with the emergence of a dynamic disorder, which characterizes the conformational transition of amyloid- $\beta$ . Thus, we conclude that memory effects play an important role in the kinetics of the conformational transitions of proteins. Results for the FEP obtained from these simulations reveal that the unfold–misfold transition of amyloid- $\beta$  is a two-state process where the unfolded and misfolded states are described as two wells separated by a free energy barrier. The TPTD computed from these simulations is compared with the theoretically obtained results that provide the frequency and height of the potential barrier for the unfold–misfold transition of amyloid- $\beta$ . The high free energy barrier confirms the misfolding of amyloid- $\beta$ . While the TPTD increases with a decrease in the width of the transition region and an increase in the frictional coefficient, the MTPT increases with the width of the transition region.

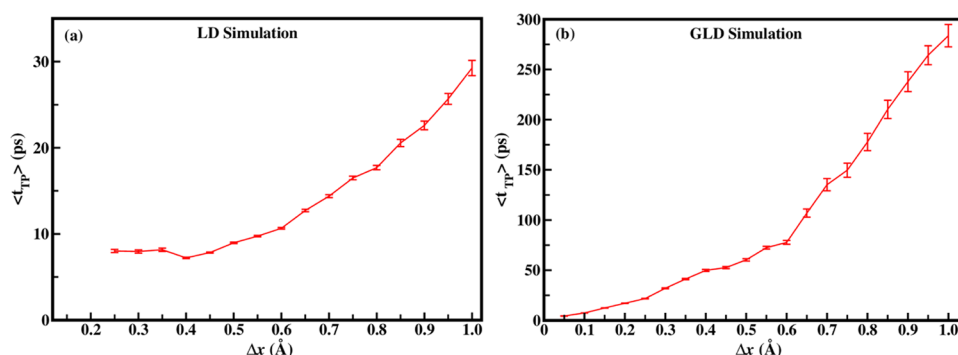


**Figure 9.** MTPT,  $\langle t_{TP} \rangle$ , versus  $\Delta x$  ( $\Delta x = x_M - x_U$ ) for the (a) LD simulation and (b) GLD simulation at fixed value  $\gamma = 1.0 \text{ ps}^{-1}$ . The error bars show the standard errors obtained while averaging over the mean time of crossing between two boundaries at different time steps.

These findings offer an insight into the dynamics of the unfold–misfold transition of this protein.

## ■ ASSOCIATED CONTENT

### Supporting Information

The Supporting Information is available free of charge at <https://pubs.acs.org/doi/10.1021/acsomega.1c00516>.

$R_g$  and RMSD of amyloid- $\beta$  from the LD and GLD simulations at different values of frictional coefficient; normalized time autocorrelation function,  $C(t)$ , versus time,  $t$ ; free energy profile with varying values of the frictional coefficients,  $\gamma$ ; and TPTD and MTPT obtained from the MD simulation for the conformational transition of A $\beta$  (PDF)

(PDF)

## ■ AUTHOR INFORMATION

### Corresponding Author

Parbati Biswas – Department of Chemistry, University of Delhi, Delhi 110007, India; [orcid.org/0000-0001-7709-2263](https://orcid.org/0000-0001-7709-2263); Phone: +91-11-2766-6646; Email: [pbiswas@chemistry.du.ac.in](mailto:pbiswas@chemistry.du.ac.in)

### Author

Vishal Singh – Department of Chemistry, University of Delhi, Delhi 110007, India

Complete contact information is available at:

<https://pubs.acs.org/doi/10.1021/acsomega.1c00516>

### Notes

The authors declare no competing financial interest.

## ■ ACKNOWLEDGMENTS

The authors gratefully acknowledge DST-SERB, India (EMR/2016/006619) for financial support and SCFBio (IIT, Delhi) for providing adequate supercomputing facility. V.S. acknowledges CSIR, India for providing financial assistance in the form of SRF (09/045(1410)/2016-EMR-I).

## ■ REFERENCES

- (1) Dong, M.; Husale, S.; Sahin, O. Determination of protein structural flexibility by microsecond force spectroscopy. *Nat. Nanotechnol.* **2009**, *4*, 514–517.
- (2) Ratner, M. A. Biomolecular processes in the fast lane. *Proc. Natl. Acad. Sci. U.S.A.* **2001**, *98*, 387–389.
- (3) Anandakrishnan, R.; Drozdetski, A.; Walker, R. C.; Onufriev, A. V. Speed of conformational change: comparing explicit and implicit

solvent molecular dynamics simulations. *Biophys. J.* **2015**, *108*, 1153–1164.

(4) Biswas, P. Theoretical and Computational Advances in Protein Misfolding. In *Advances in Protein Chemistry and Structural Biology*; Elsevier, 2020; pp 1–31.

(5) Singh, V.; Biswas, P. Estimating the mean first passage time of protein misfolding. *Phys. Chem. Chem. Phys.* **2018**, *20*, 5692–5698.

(6) Zaccai, G. How soft is a protein? A protein dynamics force constant measured by neutron scattering. *Science* **2000**, *288*, 1604–1607.

(7) Ramanathan, A.; Savol, A.; Burger, V.; Chennubhotla, C. S.; Agarwal, P. K. Protein conformational populations and functionally relevant substates. *Acc. Chem. Res.* **2014**, *47*, 149–156.

(8) Chung, H. S.; Louis, J. M.; Eaton, W. A. Experimental determination of upper bound for transition path times in protein folding from single-molecule photon-by-photon trajectories. *Proc. Natl. Acad. Sci. U.S.A.* **2009**, *106*, 11837–11844.

(9) Shaw, D. E.; Maragakis, P.; Lindorff-Larsen, K.; Piana, S.; Dror, R. O.; Eastwood, M. P.; Bank, J. A.; Jumper, J. M.; Salmon, J. K.; Shan, Y.; Wriggers, W. Atomic-level characterization of the structural dynamics of proteins. *Science* **2010**, *330*, 341–346.

(10) Karplus, M.; Kuriyan, J. Molecular dynamics and protein function. *Proc. Natl. Acad. Sci. U.S.A.* **2005**, *102*, 6679–6685.

(11) Xu, Y.; Shen, J.; Luo, X.; Zhu, W.; Chen, K.; Ma, J.; Jiang, H. Conformational transition of amyloid  $\beta$ -peptide. *Proc. Natl. Acad. Sci. U.S.A.* **2005**, *102*, 5403–5407.

(12) Baruah, A.; Biswas, P. Globular-disorder transition in proteins: a compromise between hydrophobic and electrostatic interactions. *Phys. Chem. Chem. Phys.* **2016**, *18*, 23207–23214.

(13) Chong, S.-H.; Park, M.; Ham, S. Structural and thermodynamic characteristics that seed aggregation of amyloid- $\beta$  protein in water. *J. Chem. Theory Comput.* **2012**, *8*, 724–734.

(14) Lee, C.; Ham, S. Characterizing amyloid-beta protein misfolding from molecular dynamics simulations with explicit water. *J. Comput. Chem.* **2011**, *32*, 349–355.

(15) Flöck, D.; Colacino, S.; Colombo, G.; Di Nola, A. Misfolding of the amyloid  $\beta$ -protein: A molecular dynamics study. *Proteins: Struct., Funct., Bioinf.* **2006**, *62*, 183–192.

(16) Ozmaian, M.; Makarov, D. E. Transition path dynamics in the binding of intrinsically disordered proteins: A simulation study. *J. Chem. Phys.* **2019**, *151*, No. 235101.

(17) Chung, H. S. Transition path times measured by single-molecule spectroscopy. *J. Mol. Biol.* **2018**, *430*, 409–423.

(18) Neupane, K.; Hoffer, N. Q.; Woodside, M. Measuring the local velocity along transition paths during the folding of single biological molecules. *Phys. Rev. Lett.* **2018**, *121*, No. 018102.

(19) Kramers, H. A. Brownian motion in a field of force and the diffusion model of chemical reactions. *Physica* **1940**, *7*, 284–304.

(20) Hänggi, P.; Talkner, P.; Borkovec, M. Reaction-rate theory: fifty years after Kramers. *Rev. Mod. Phys.* **1990**, *62*, 251–341.

- (21) Grote, R. F.; Hynes, J. T. The stable states picture of chemical reactions. II. Rate constants for condensed and gas phase reaction models. *J. Chem. Phys.* **1980**, *73*, 2715–2732.
- (22) Peters, B. *Reaction Rate Theory and Rare Events*; Elsevier Amsterdam, 2017.
- (23) Case, D. A.; Ben-Shalom, I. Y.; Brozel, S. R.; Cerutti, D. S.; Cheatham, T. E., III; Cruzeiro, V. W. D.; Darden, T. A.; Duke, R. E.; Ghoreishi, D.; Gilson, M. K. et al. *AMBER 18*; University of California: San Francisco: San Francisco, 2018.
- (24) Lindorff-Larsen, K.; Piana, S.; Palmo, K.; Maragakis, P.; Klepeis, J. L.; Dror, R. O.; Shaw, D. E. Improved side-chain torsion potentials for the Amber ff99SB protein force field. *Proteins: Struct., Funct., Bioinf.* **2010**, *78*, 1950–1958.
- (25) Shao, Q.; Zhu, W. Assessing AMBER force fields for protein folding in an implicit solvent. *Phys. Chem. Chem. Phys.* **2018**, *20*, 7206–7216.
- (26) Pastor, R. W.; Brooks, B. R.; Szabo, A. An analysis of the accuracy of Langevin and molecular dynamics algorithms. *Mol. Phys.* **1988**, *65*, 1409–1419.
- (27) Bashford, D.; Case, D. A. Generalized born models of macromolecular solvation effects. *Annu. Rev. Phys. Chem.* **2000**, *51*, 129–152.
- (28) Onufriev, A. Chapter 7 - Implicit solvent models in molecular dynamics simulations: A brief overview. *Annu. Rep. Comput. Chem.* **2008**, *4*, 125–137.
- (29) Weiser, J.; Shenkin, P. S.; Still, W. C. Approximate atomic surfaces from linear combinations of pairwise overlaps (LCPO). *J. Comput. Chem.* **1999**, *20*, 217–230.
- (30) Ryckaert, J.-P.; Ciccotti, G.; Berendsen, H. J. Numerical integration of the cartesian equations of motion of a system with constraints: molecular dynamics of n-alkanes. *J. Comput. Phys.* **1977**, *23*, 327–341.
- (31) Kubo, R.; Toda, M.; Hashitsume, N. *Statistical Physics II: Nonequilibrium Statistical Mechanics*; Springer-Verlag, Berlin, Heidelberg, 1985; Vol. 31.
- (32) Nitzan, A. *Chemical Dynamics in Condensed Phases: Relaxation, Transfer and Reactions in Condensed Molecular Systems*; Oxford University Press, Oxford, 2006.
- (33) Kubo, R. The fluctuation-dissipation theorem. *Rep. Prog. Phys.* **1966**, *29*, 255–284.
- (34) Berendsen, H. J.; Postma, J. v.; van Gunsteren, W. F.; DiNola, A.; Haak, J. R. Molecular dynamics with coupling to an external bath. *J. Chem. Phys.* **1984**, *81*, 3684–3690.
- (35) Darden, T.; York, D.; Pedersen, L. Particle mesh Ewald: An N.log(N) method for Ewald sums in large systems. *J. Chem. Phys.* **1993**, *98*, 10089–10092.
- (36) Triguero, L.; Singh, R.; Prabhakar, R. Comparative molecular dynamics studies of wild-type and oxidized forms of full-length Alzheimer amyloid  $\beta$ -peptides A $\beta$  (1–40) and A $\beta$  (1–42). *J. Phys. Chem. B* **2008**, *112*, 7123–7131.
- (37) Wigner, E. The transition state method. *Trans. Faraday Soc.* **1938**, *34*, 29–41.
- (38) Miller, W. H. Unified statistical model for “complex” and “direct” reaction mechanisms. *J. Chem. Phys.* **1976**, *65*, 2216–2223.
- (39) Eyring, H. The activated complex in chemical reactions. *J. Chem. Phys.* **1935**, *3*, 107–115.
- (40) Hummer, G. From transition paths to transition states and rate coefficients. *J. Chem. Phys.* **2004**, *120*, 516–523.
- (41) Geissler, P. L.; Dellago, C.; Chandler, D. Kinetic pathways of ion pair dissociation in water. *J. Phys. Chem. B* **1999**, *103*, 3706–3710.
- (42) Chandler, D. Statistical mechanics of isomerization dynamics in liquids and the transition state approximation. *J. Chem. Phys.* **1978**, *68*, 2959–2970.
- (43) Chandler, D. *Introduction to Modern Statistical Mechanics*; Oxford University Press, Oxford, UK, 1987.
- (44) Straub, J. E.; Hsu, D. A.; Berne, B. J. On determining reaction kinetics by molecular dynamics using absorbing barriers. *J. Phys. Chem. A* **1985**, *89*, 5188–5191.
- (45) Mosell, T.; Schrimpf, G.; Hahn, C.; Brickmann, J. Cage-to-cage jumps of xenon in zeolite NaY: Transmission coefficients from molecular dynamics simulations. *J. Phys. Chem. B* **1996**, *100*, 4571–4581.
- (46) Straub, J. E.; Borkovec, M.; Berne, B. J. Non-Markovian activated rate processes: Comparison of current theories with numerical simulation data. *J. Chem. Phys.* **1986**, *84*, 1788–1794.
- (47) Bag, B. C.; Hu, C.-K.; Li, M. S. Colored noise, folding rates and departure from Kramers’ behavior. *Phys. Chem. Chem. Phys.* **2010**, *12*, 11753–11762.
- (48) Min, W.; Xie, X. S. Kramers model with a power-law friction kernel: Dispersed kinetics and dynamic disorder of biochemical reactions. *Phys. Rev. E* **2006**, *73*, No. 010902.
- (49) Luo, G.; Andricioaei, I.; Xie, X. S.; Karplus, M. Dynamic distance disorder in proteins is caused by trapping. *J. Phys. Chem. B* **2006**, *110*, 9363–9367.
- (50) Min, W.; Luo, G.; Cherayil, B. J.; Kou, S.; Xie, X. S. Observation of a power-law memory kernel for fluctuations within a single protein molecule. *Phys. Rev. Lett.* **2005**, *94*, No. 198302.
- (51) Mori, T.; Saito, S. Molecular mechanism behind the fast folding/unfolding transitions of villin headpiece subdomain: Hierarchy and heterogeneity. *J. Phys. Chem. B* **2016**, *120*, 11683–11691.
- (52) McAllister, C.; Karymov, M. A.; Kawano, Y.; Lushnikov, A. Y.; Mikheikin, A.; Uversky, V. N.; Lyubchenko, Y. L. Protein interactions and misfolding analyzed by AFM force spectroscopy. *J. Mol. Biol.* **2005**, *354*, 1028–1042.
- (53) Maity, S.; Lyubchenko, Y. L. AFM Probing of Amyloid-Beta 42 Dimers and Trimers. *Front. Mol. Biosci.* **2020**, *7*, No. 69.
- (54) Laleman, M.; Carlon, E.; Orland, H. Transition path time distributions. *J. Chem. Phys.* **2017**, *147*, No. 214103.
- (55) Chaudhury, S.; Makarov, D. E. A harmonic transition state approximation for the duration of reactive events in complex molecular rearrangements. *J. Chem. Phys.* **2010**, *133*, No. 034118.
- (56) Zhang, B. W.; Jasnow, D.; Zuckerman, D. M. Transition-event durations in one-dimensional activated processes. *J. Chem. Phys.* **2007**, *126*, No. 074504.
- (57) Caraglio, M.; Put, S.; Carlon, E.; Vanderzande, C. The influence of absorbing boundary conditions on the transition path time statistics. *Phys. Chem. Chem. Phys.* **2018**, *20*, 25676–25682.